small
methods

Supporting Information

for *Small Methods*, DOI 10.1002/smtd.202400070

# Averting $H^+$-Mediated Charge Storage Chemistry Stabilizes the High Output Voltage of $LiMn_2O_4$-Based Aqueous Battery

*Abhirup Bhadra, S. Swathilakshmi, Uttam Mittal, Neeraj Sharma*, Gopalakrishnan Sai Gautam* and Dipan Kundu**

# Supporting Information for

# Averting $H^+$-Mediated Charge Storage Stabilizes the High Output Voltage of $LiMn_2O_4$-Based Aqueous Battery

*Abhirup Bhadra*[a], *S. Swathilakshmi*[b], *Uttam Mittal*[c], *Neeraj Sharma*[c,#], *Gopalakrishnan Sai Gautam*[b,#] *and Dipan Kundu*[a,d,*]

[a] School of Chemical Engineering, UNSW Sydney, Kensington, NSW 2052, Australia

[b] Department of Materials Engineering, Indian Institute of Science, Bengaluru 560012, India

[c] School of Chemistry, UNSW Sydney, Kensington, NSW 2052, Australia

[d] School of Mechanical and Manufacturing Engineering, UNSW Sydney, Kensington, NSW 2052, Australia

#Corresponding author; Email: neeraj.sharma@unsw.edu.au

#Corresponding author; Email saigautamg@iisc.ac.in

*Corresponding author; Email: d.kundu@unsw.edu.au

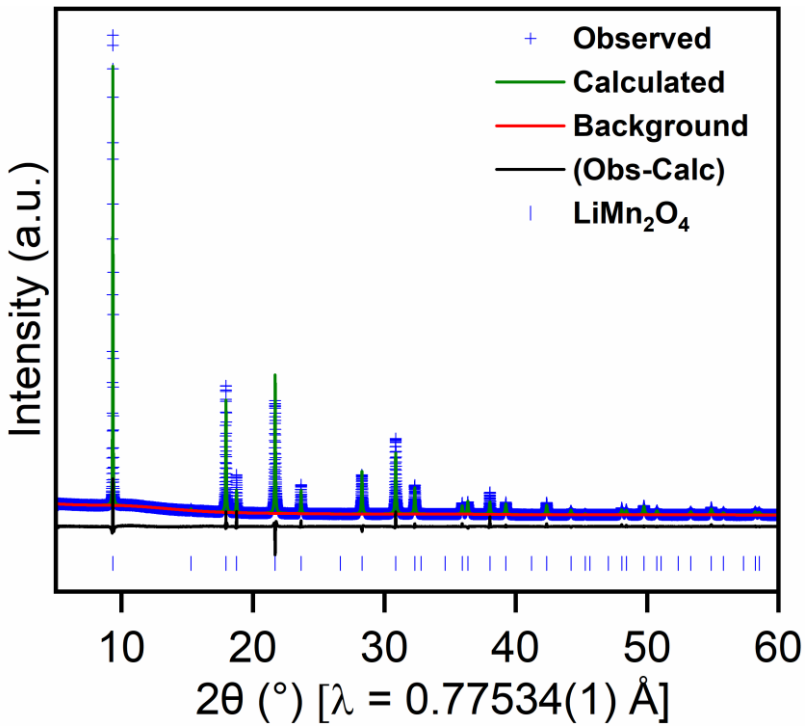


**Figure S1**. Rietveld refinement ($R_{wp}$: 5.9%) of the structural model with synchrotron powder XRD data of pristine commercially obtained $LiMn_2O_4$ spinel using cubic spinel (*Fd*-3*mZ*) $LiMn_2O_4$ structural model (ICSD #11273)

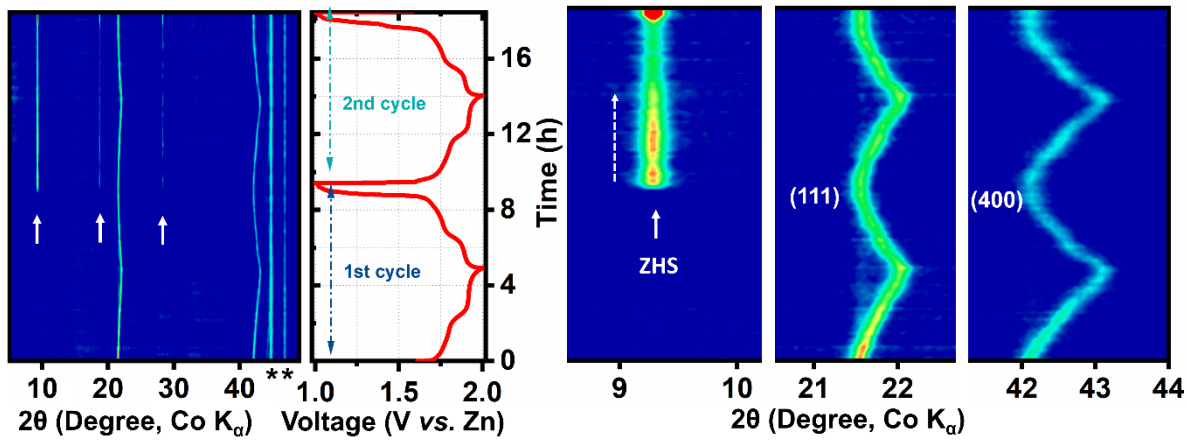


**Figure S2**. *Operando* XRD contour plot for the first two cycles for $LiMn_2O_4$ in a $LiMn_2O_4$||Zn cell with the 1-1 $Li_2SO_4$-$ZnSO_4$ electrolyte cycled at a 0.2C rate and the corresponding galvanostatic charge-discharge profile. The diffraction peaks for the $H^+$ intercalation byproduct ZHS are labeled with the arrows. The asterisks on the 2θ axis label the diffraction peaks arising from the operando cell body. The evolution of the (b) ZHS peak and $LiMn_2O_4$ (c) (111) peak upon charge-discharge.

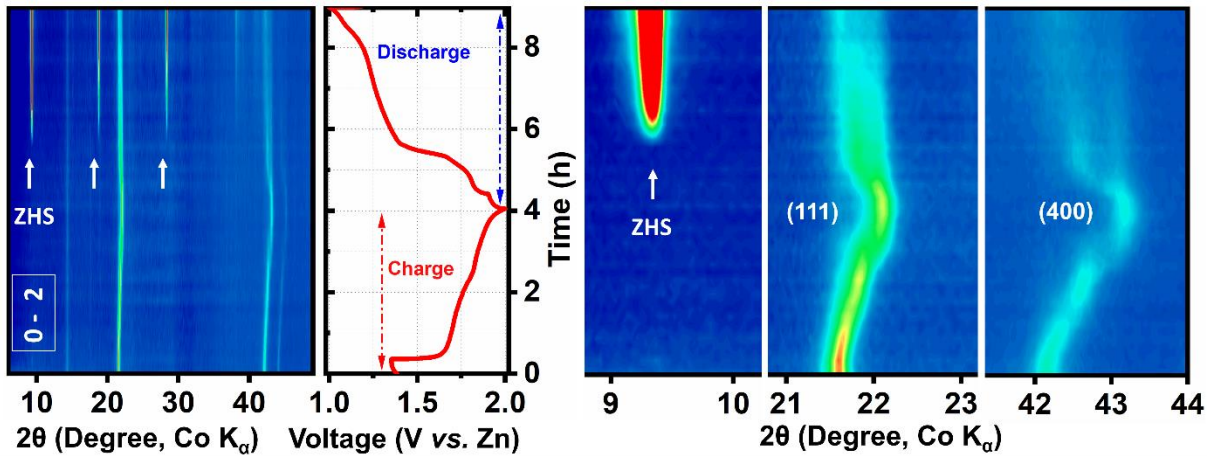


**Figure S3.** *Operando* XRD contour plot for the first two cycles for $LiMn_2O_4$ in a $LiMn_2O_4$||Zn cell with the 0-2 $Li_2SO_4$-$ZnSO_4$ electrolyte cycled at a 0.2C rate and the corresponding galvanostatic charge-discharge profile. The diffraction peaks for the $H^+$ intercalation byproduct ZHS are labeled with the arrows. The evolution of the ZHS peak and $LiMn_2O_4$ (111) and (400) peak upon charge-discharge is shown on the right.

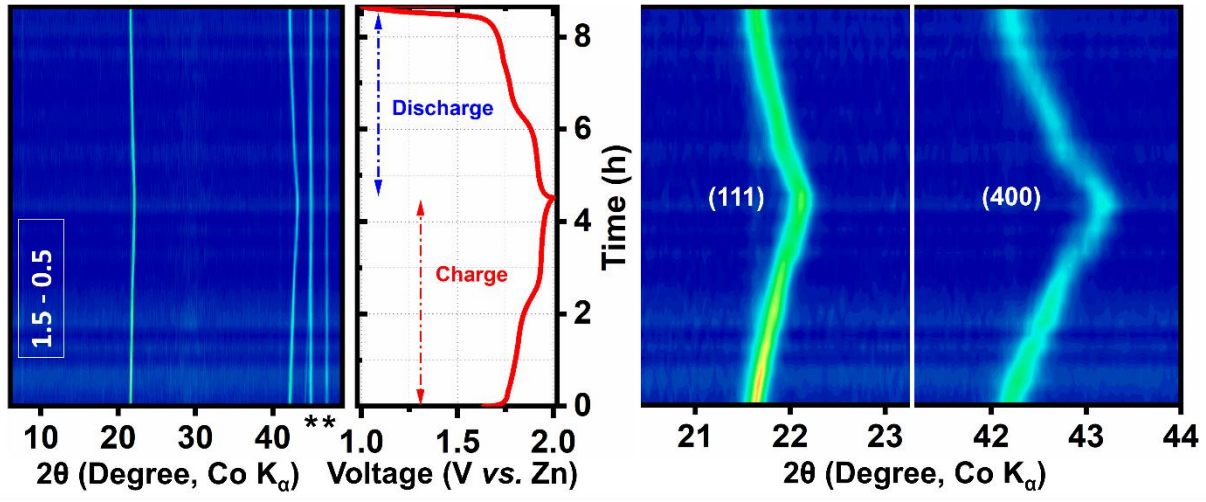


**Figure S4**. *Operando* XRD contour plot for the first two cycles for $LiMn_2O_4$ in a $LiMn_2O_4$||Zn cell with the 1.5-0.5 $Li_2SO_4$-$ZnSO_4$ electrolyte cycled at a 0.2C rate and the corresponding galvanostatic charge-discharge profile. The asterisks on the 2θ axis label the diffraction peaks arising from the operando cell body. The evolution of the $LiMn_2O_4$ (111) and (400) peaks upon charge-discharge are shown on the right.

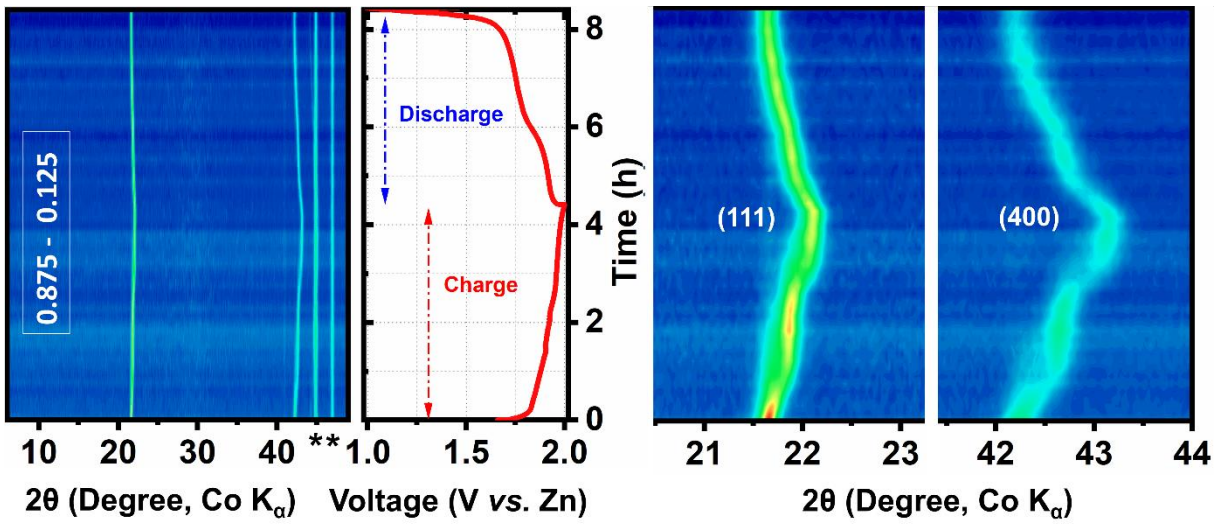


**Figure S5**. *Operando* XRD contour plot for the first two cycles for $LiMn_2O_4$ in a $LiMn_2O_4$||Zn cell with the 0.875-0.125 $Li_2SO_4$-$ZnSO_4$ electrolyte cycled at a 0.2C rate and the corresponding galvanostatic charge-discharge profile. The asterisks on the 2θ axis label the diffraction peaks arising from the operando cell body. The evolution of the $LiMn_2O_4$ (111) and (400) peaks upon charge-discharge are shown on the right.

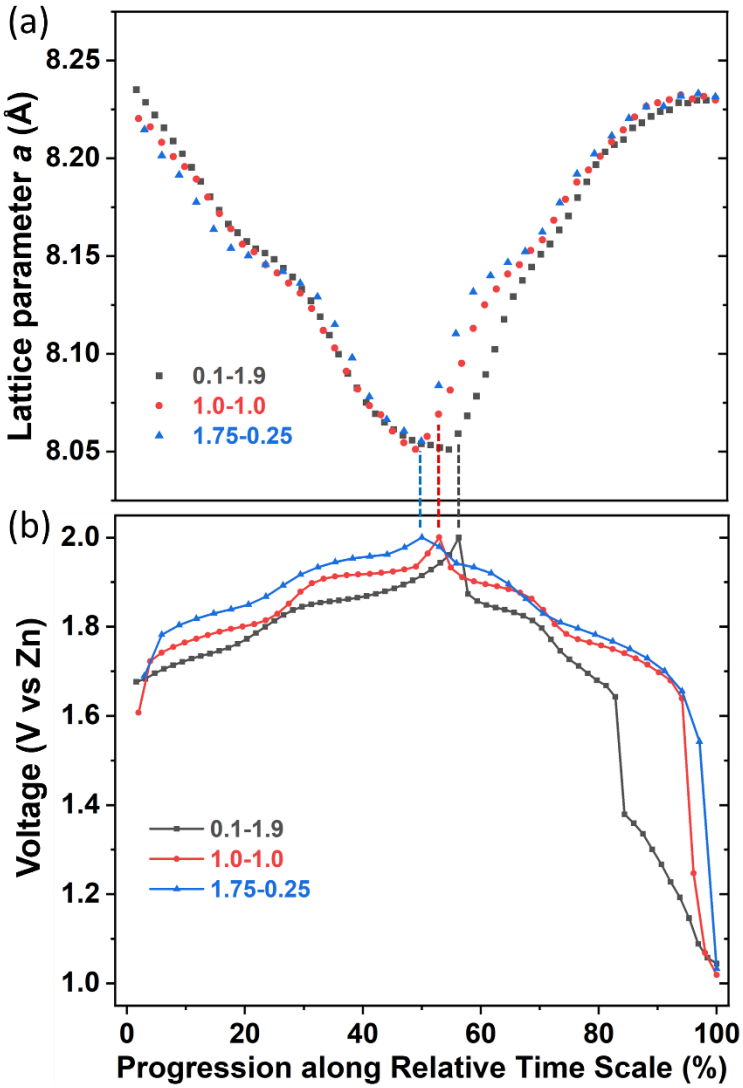


**Figure S6**. Spinel $LiMn_2O_4$ (a) ***a*** lattice parameter evolution during charge – discharge in 0.1-1.9, 1-1, and 1.75-0.25 $Li_2SO_4$-$ZnSO_4$ electrolytes and (b) the corresponding voltage profile.

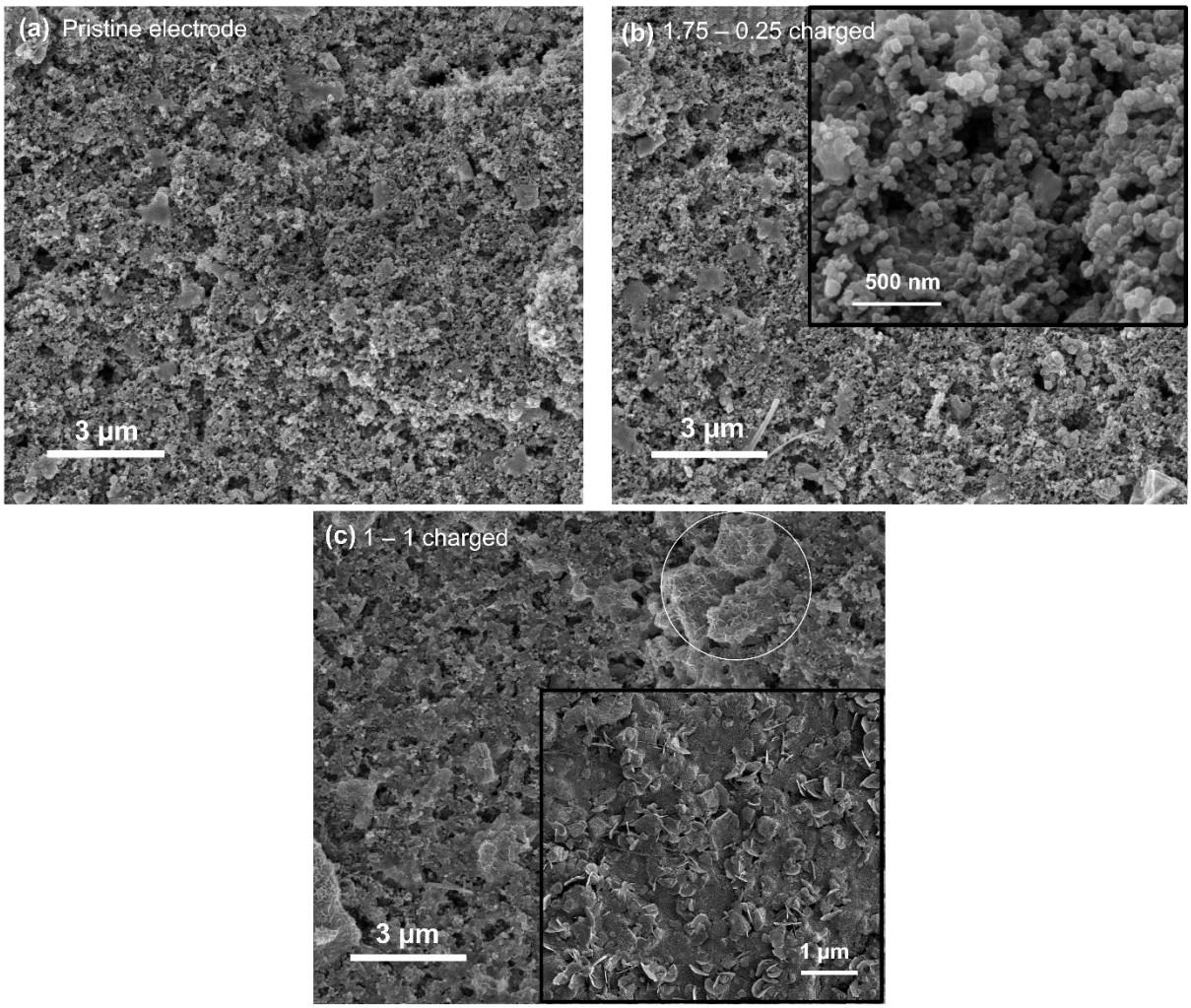


**Figure S7**. Representative SEM images for the $LiMn_2O_4$ electrode (a) at the pristine state before electrochemical cycling and after second charge in (b) 1.75-0.25 and (c) 1-1 $Li_2SO_4$-$ZnSO_4$ electrolytes. The flaky material observed in (c) is the $H^+$ intercalation byproduct that remains unreacted after charging indicating irreversibility of the $H^+$ mediated charge storage process.

**Table S1**. The lithium composition of the discharged $Li_xMn_2O_4$ cathode after cycling in 0.1-1.9, 1-1, 1.25-0.75, 1.5-0.5, 1.75-0.25, and 0.875-0.125 $Li_2SO_4$-$ZnSO_4$ electrolytes. The cathodes were cycled at a 0.1C current rate and stopped after the second discharge. The recovered cathodes were thoroughly washed with water for the composition analysis by ICP-OES. Even though hydrogen is not directly detected by ICP-OES, Zn to Mn ratio can indirectly indicate the hydrogen composition as one mole of $Zn_4SO_4(OH)_6 \cdot 5H_2O$ accumulated on the cathode surface corresponds to 6 moles of intercalated $H^+$. However, during the thorough washing of the cathodes the LDH flakes easily fall off and leads to inaccurate estimation. Therefore, Li and Mn wt% has been used to determine the Li stoichiometry in the discharged cathode and it is safe to assume that H-stoichiometry corresponds to the deficiency in Li stoichiometry.

| **Elec $Li_2SO_4$-$ZnSO_4$ (M)** | **Li** | **Mn** | **Zn** | **Li** | **Mn** | **Zn** | **$Li_xH_yMn_2O_4$** |
|---|---|---|---|---|---|---|---|
| | %wt | %wt | %wt | %wt/MW(Li) | %wt/MW(Mn) | %wt/MW(Zn) | x |
| 0.1-1.9 | 1.53 | 45.2 | 4.95 | 0.22 | 0.82 | 0.08 | **0.54** |
| 1-1 | 2.55 | 46.4 | 3.91 | 0.37 | 0.84 | 0.06 | **0.84** |
| 1.25-0.75 | 2.55 | 45.3 | 3.91 | 0.37 | 0.82 | 0.06 | **0.90** |
| 1.5-0.5 | 2.74 | 47.7 | 1.81 | 0.40 | 0.87 | 0.03 | **0.92** |
| 1.75-0.25 | 2.72 | 44.1 | 0.44 | 0.39 | 0.80 | 0.006 | **0.98** |
| 0.875-0.125 | 2.77 | 50.7 | 1.18 | 0.41 | 0.92 | 0.02 | **0.89** |

**Table S2**. Evolution of the $Li_xMn_2O_4$ cathode composition as a function of the discharge voltage after cycling in 1-1 and 1.75-0.25 $Li_2SO_4$-$ZnSO_4$ electrolytes. The cathodes were cycled at a 0.1C current rate and stopped at the noted voltages. The recovered cathodes were thoroughly washed with water for the composition analysis by ICP-OES.

| **Voltage (w.r.t. Zn)** | **1.75 - 0.25 $Li_2SO_4$-$ZnSO_4$ (M)** | **1-1 $Li_2SO_4$-$ZnSO_4$ (M)** |
|---|---|---|
| **Pristine** | $Li_{0.99}Mn_2O_4$ | $Li_{0.99}Mn_2O_4$ |
| **Charged** | $Li_{0.15}Mn_2O_4$ | $Li_{0.13}Mn_2O_4$ |
| **1.85 V (Discharged)** | $Li_{0.54}Mn_2O_4$ | $Li_{0.57}Mn_2O_4$ |
| **1.75 V (Discharged)** | $Li_{0.86}Mn_2O_4$ | $Li_{0.72}Mn_2O_4$ |
| **1.5 V (Discharged)** | $Li_{0.94}Mn_2O_4$ | $Li_{0.83}Mn_2O_4$ |
| **1.0 V (Discharged)** | $Li_{0.98}Mn_2O_4$ | $Li_{0.84}Mn_2O_4$ |

**Table S3**. The pH of the $Li_2SO_4$-$ZnSO_4$ electrolytes.

| **$Li_2SO_4$** | **$ZnSO_4$** | **pH** |
|---|---|---|
| 0.875 | 0.125 | 5.65 |
| 1.75 | 0.25 | 5.4 |
| 1.5 | 0.5 | 5.3 |
| 1.25 | 0.75 | 5 |
| 1.0 | 1.0 | 4.7 |
| 0.1 | 1.9 | 4.6 |
| 0.0 | 2.0 | 4.45 |

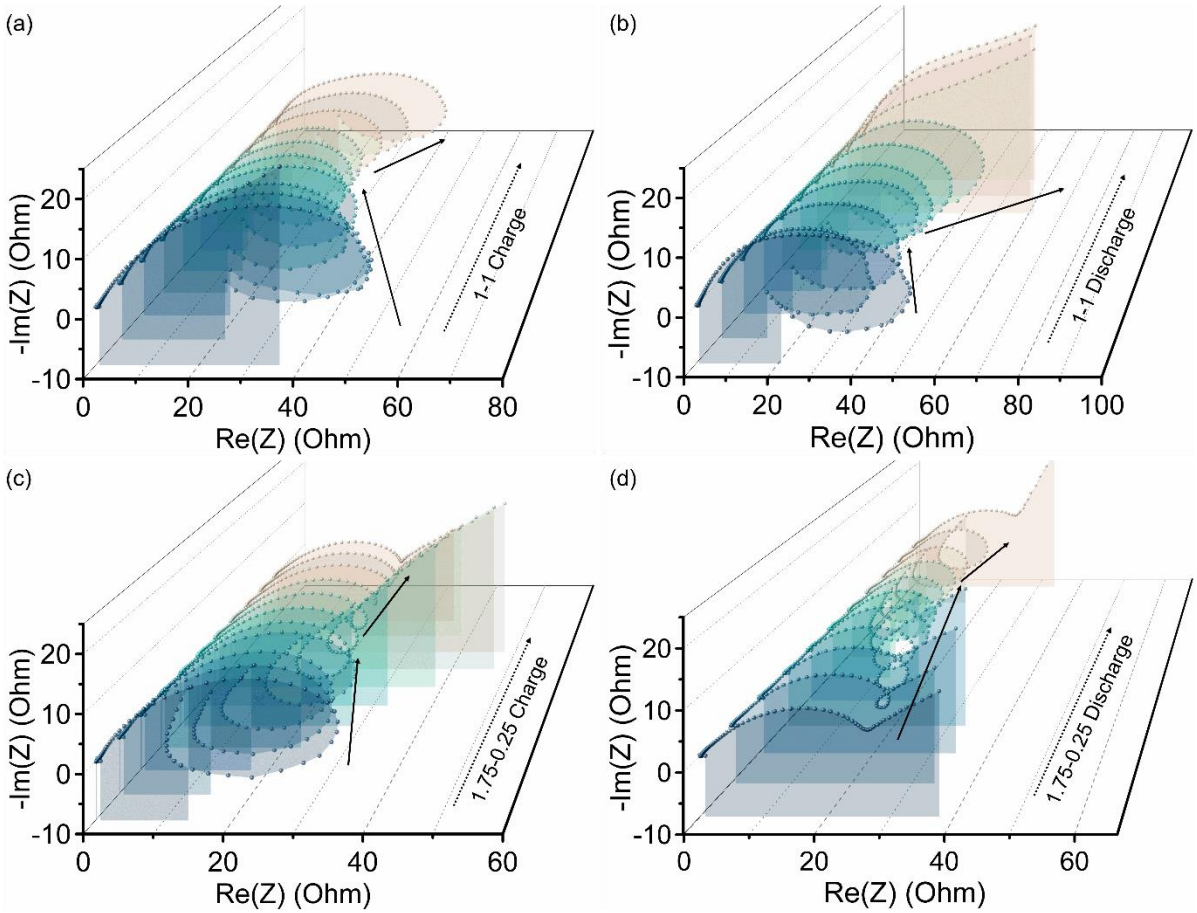


**Figure S8**. Nyquist impedance evolution for the $LiMn_2O_4$ working electrode as a function of the state of charge during the first charge-discharge cycles in (a, b) 1-1 and (c, d) 1.75-0.25 $Li_2SO_4$-$ZnSO_4$ electrolyte, obtained by employing a 3-electrode cell with Zn as counter and reference electrodes. The evolution in the two cells is comparable except for toward the end of the discharge. While in the 1.75-0.25 electrolyte, the charge transfer resistance ($R_{ct}$; high-mid frequency semicircle) returns back to the pre-charge value (~40 Ohm) at the end of discharge with only a little rise in $R_{ct}$ at the end after an initial decline, for 1-1 the $R_{ct}$ rises significantly at the end of the discharge (to over 100 Ohm, as can be extrapolated) when $H^+$ intercalation is dominant. This indicates a rather high charge transfer barrier for $H^+$ intercalation or sluggish nature of the $H^+$ intercalation.

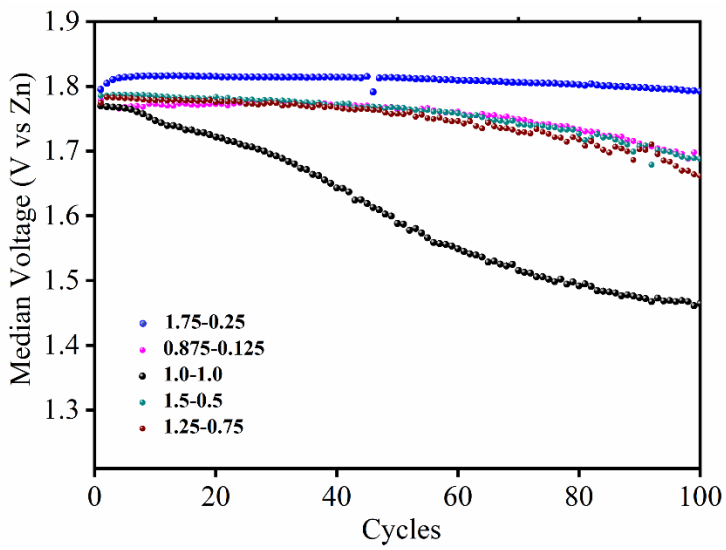


**Figure S9**. The median discharge voltage evolution as a function of cycling for electrolytes with different $Li^{+}$ to $Zn^{2}$+ ratio in the electrolyte.

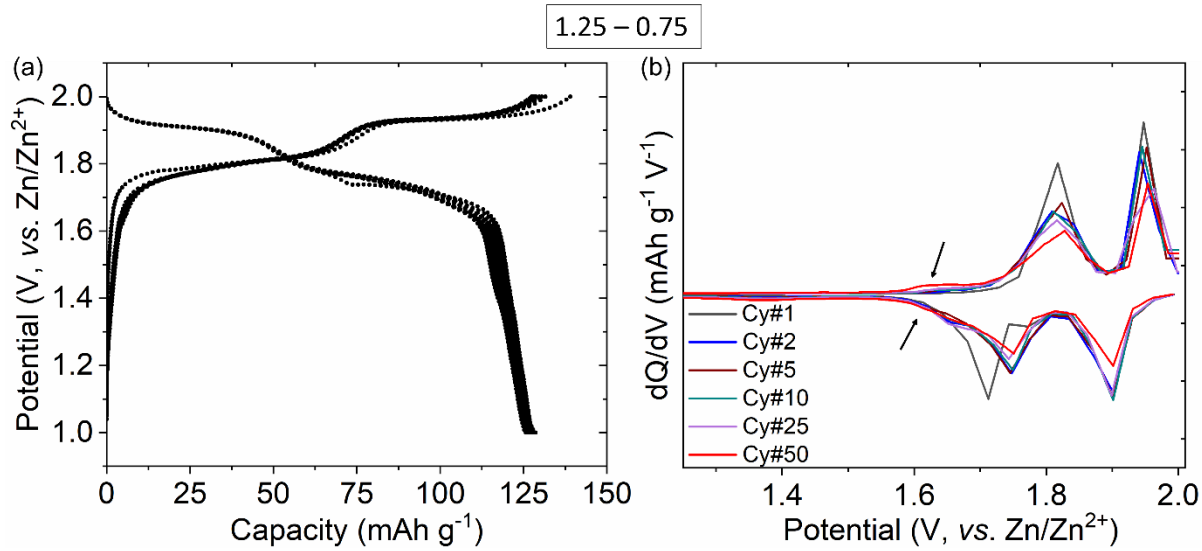


**Figure S10**. (a) The galvanostatic charge-discharge profile for the $LiMn_2O_4$||Zn cell with the 1.25-0.25 electrolyte and (b) the corresponding differential capacity profile during the first ten cycles. The arrows in (b) points to the peaks arising at low voltages with increasing cycle number.

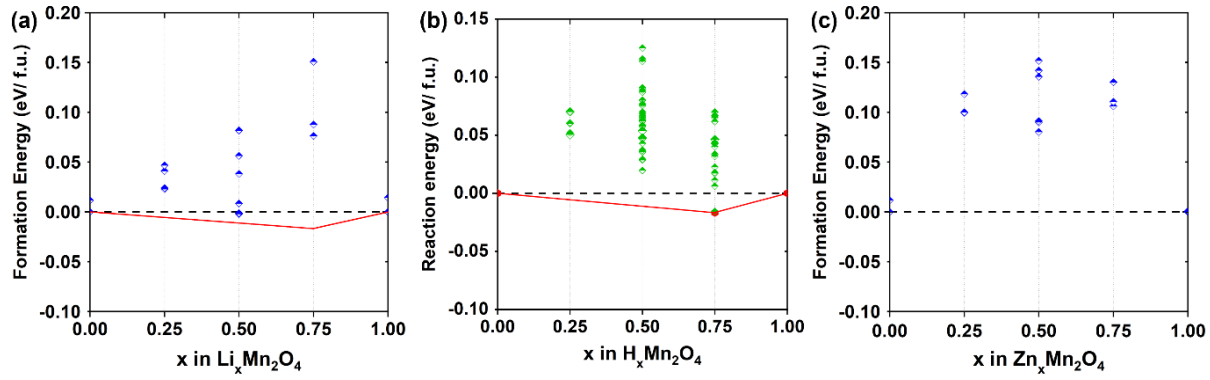


**Figure S11**. The ground-state hull of (a) Li in $LixMn_2O_4$; (b) H in $HxMn_2O_4$; (c) Zn in $ZnxMn_2O_4$. The formation energy per formula unit has been plotted with respect to the intercalating ion concentration in the system, denoted by x.

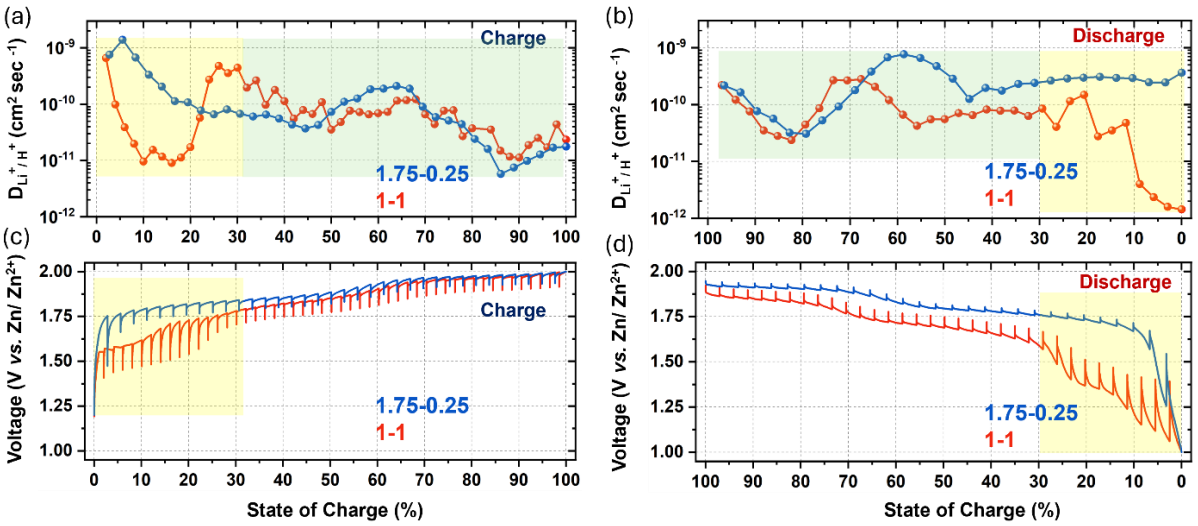


**Figure S12**. Diffusion coefficients during (a) charge and (b) discharge as calculated by applying galvanostatic intermittent titration technique (GITT). (c, d) The corresponding GITT profiles. The GITT experiment was performed after a charge-discharge cycle at a 0.3C rate.

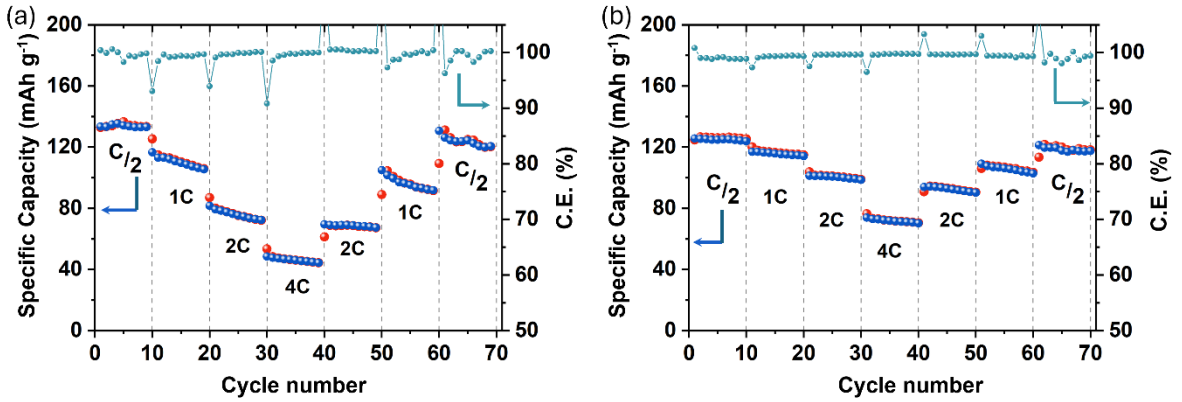


**Figure S13**. Specific capacity variation for the $LiMn_2O_4$||Zn cell as a function of the current rate with (a) 1-1 and (b) 1.75-0.25 electrolyte.

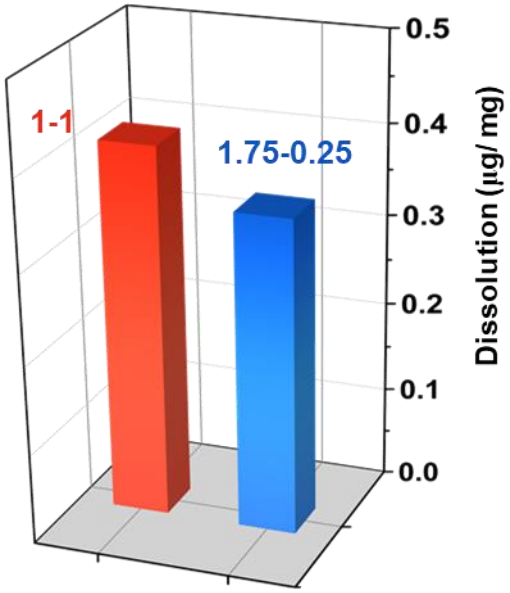


**Figure S14**. Mn dissolution (µg per mg or 1000 µg of the active cathode) detected by ICP-OES analysis of the electrolyte collected after 30 charge-discharge cycles. A cathode loading of ~5 mg $cm^{-2}$ was applied here.

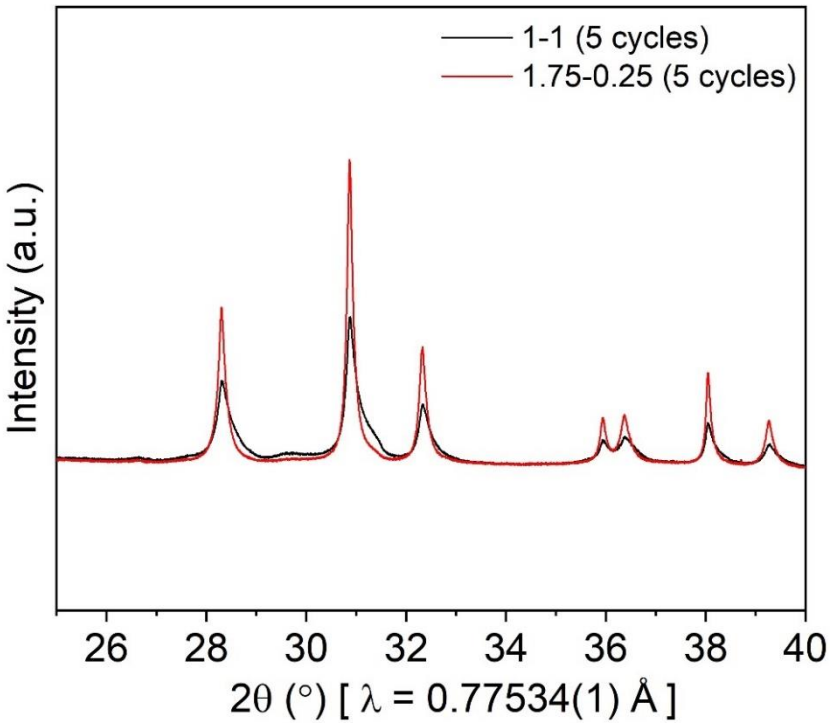


**Figure S15**. Comparison of the synchrotron XRD data for the $LiMn_2O_4$ electrode after five charge-discharge cycles in 1-1 vis-à-vis 1.75-0.25 electrolyte.

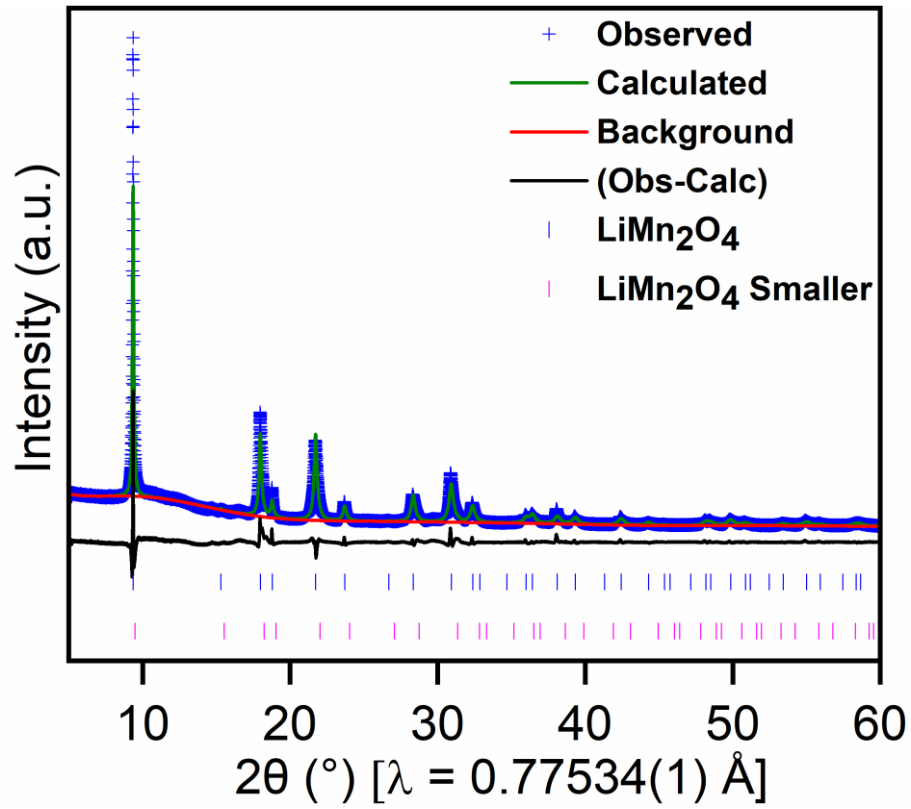


**Figure S16.** Rietveld refinement of structural models with synchrotron powder XRD data of the $LiMn_2O_4$ electrode cycled in the 1-1 electrolyte for 50 cycles. The symbols used in the plot are explained inside the figure.

**Table S4.** Rietveld-refined structural parameters for the postmortem samples. Refinements were performed using synchrotron XRD data. $LiMn_2O_4$ S refers to the $LiMn_2O_4$ smaller phase noted in the manuscript and the $L_y$ term is the Lorentzian term used to define the peak profiles for the refinements. * denotes fixed in final refinements.

| Sample | Lattice parameter $LiMn_2O_4$ | O position | Lattice parameter $LiMn_2O_4$ S | Phase fraction ($LiMn_2O_4$) | Phase fraction ($LiMn_2O_4$ S) | $L_y$ | $R_{wp}$ (%) |
|---|---|---|---|---|---|---|---|
| 1-1 5 cy | 8.2353(1) | 0.2366(1) | - | - | - | 83.4 | 6.8 |
| 1-1 50 cy | 8.2244(2) | 0.2366* | 8.112(5) | 0.973(2) | 0.027(2) | 119.2 | 6.9 |
| 1-1 100 cy | 8.2344(2) | 0.2360* | 8.153(1) | 0.908(3) | 0.092(3) | 99.5 | 6.6 |
| 1.75-0.25 5 cy | 8.2391(1) | 0.2364(1) | - | - | - | 59.2 | 6.7 |
| 1.75-0.25 50 cy | 8.2378(1) | 0.2357(1) | - | - | - | 58.7 | 6.1 |
| 1.75-0.25 100 cy _ $2^{nd}$ phase | 8.2375(1) | 0.2370* | 8.1392(4) | 0.990(2) | 0.010(2) | 68.5 | 6.3 |
| Pristine | 8.2413(1) | 0.2360(1) | | | | 23.1 | 5.9 |